Analysis and Dark Matter Search Results from DEAP-3600 with 231 Live Days at SNOLAB

S Westerdale for the DEAP-3600 Collaboration

Department of Physics, Carleton University, Ottawa Ontario K1S 5B6, Canada

E-mail: shawest@physics.carleton.ca

Abstract. DEAP-3600 is a dark matter direct detection experiment in SNOLAB (Sudbury, Canada). This single-phase detector consists of 3.3 tonnes of liquid argon, viewed by an array of 255 photomultiplier tubes through 50 cm of acrylic. The collaboration has recently released dark matter search results from the first year of running (Nov. 2016 to Oct. 2017), with a total live time of 231 days. These proceedings detail the analysis underlying these results, including the development of a background model, which constitute the most sensitive search performed with a LAr target for WIMPs with a mass greater than 30 GeV.

1. Introduction

DEAP-3600 is a dark matter direction detection experiment at SNOLAB, in Sudbury, Canada. The detector (see [1]), consists of 3279 kg of liquid argon (LAr) contained in a 5 cm-thick acrylic vessel (AV), which is viewed by 255 PMTs via 45 cm-long acrylic light guides (LGs). The LGs, and the filler blocks (FBs) between them, provide thermal insulation and neutron shielding. The inner surface of the AV is coated in TPB, which converts the 128 nm LAr scintillation light to a visible spectrum, peaked at 420 nm, where it can be detected. A layer of gaseous argon (GAr) sits at the top of the AV and fills the neck, where a cooling coil condenses GAr into the AV, passing over flow guides (FGs) at the base of the neck. Wavelength-shifting fibers wrap around the base of the neck and couple to 4 PMTs, constituting the neck veto. The detector is in a stainless steel sphere inside a $\sim$300 t water Cherenkov muon veto.

The detector started filling in June 2016, and was stable from August 7–17. Data collected during this period were used in the first WIMP search, which saw no candidate WIMP events [2]. After this period, a seal failure in the neck required that the detector be drained and refilled to a lower level. This refill finished on October 24, 2016, and the detector has been stable since. The results presented here are based on a non-blind analysis of the data collected from November 4, 2016 to Octber 31, 2017, with a total of 230.63 live-days. These results are discussed in more detail in [3]. Data collected in 2018 onward are blinded for a future analysis.

2. Event reconstruction

Energy is estimated by counting photoelectrons (PE) in a 10 µs window. A Bayesian algorithm is used to count PE and remove afterpulsing (AP), based on [4] with prior distributions added for AP time and charge. These distributions and the single PE charge distribution are measured *in situ* with a light insertion system. These calibrations (detailed in [5]) are performed regularly so that changes in these distributions can be detected and accounted for.

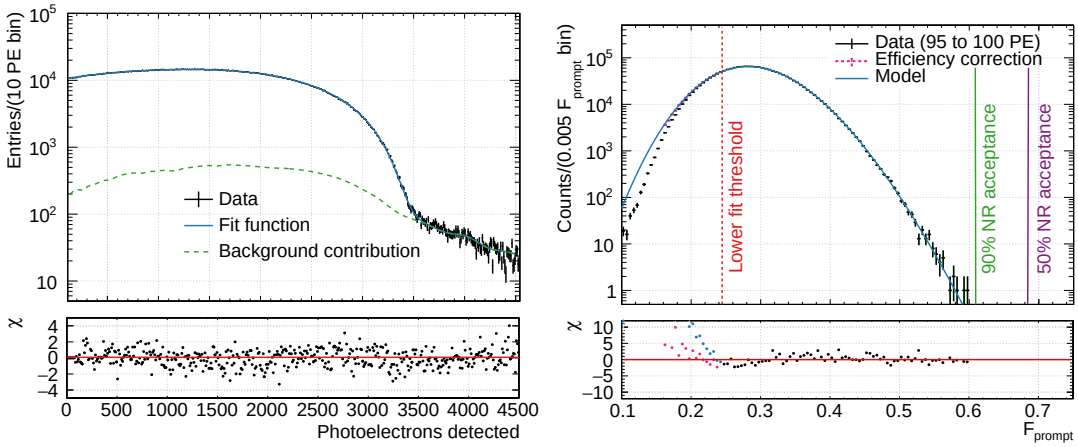

Figure 1. (Left) The observed PE distribution for ^{39}Ar events, including the detector response model fit to the spectrum for energy calibration. (Right) The F_{prompt} distribution in the lowest 1 keV_{ee} bin used for the WIMP search, with the PSD model fit to it.

Figure 1 shows the PE distribution observed in this dataset for ERs below 4500 PE. Events in this PE range are dominated by β-decays of ^{39}Ar, which is present in atmospherically-derived Ar at ∼1 Bq/kg and decays with a (565 ± 5) keV endpoint. A parameterized response function is used to fit a theoretical spectrum to the observed one, giving a light yield of (6.1 ± 0.4) PE/keV_{ee}.

Pulse shape discrimination (PSD) allows one to separate electronic recoils (ERs), with a slow scintillation time profile, from faster nuclear recoils (NRs) by counting the fraction of PE detected in the first 60 ns of an event (called F_{prompt}). The PSD model is an empirical function of F_{prompt} whose parameters vary smoothly with PE, fit to ^{39}Ar data as described in [3]. Figure 1 shows that the model fits the data well and predicts a leakage fraction of $2.8^{+1.3}_{-0.6} \times 10^{-7}$ ($1.2^{+0.7}_{-0.3} \times 10^{-9}$) with 90 % (50 %) NR acceptance in the lowest 1 keV_{ee} used for the WIMP search. These models are combined with NR quenching factor and pulse shape measurements from [6] to produce the NR models, which are validated by comparing AmBe neutron calibration data to simulation.

Two position reconstruction algorithms are used. The PE-based algorithm determines the most likely vertex given the number of PE seen by each PMT, and the time residual-based algorithm uses the times-of-flight for photons detected in the first 40 ns of an event. The PE-based algorithm was found to perform better, and is therefore used for fiducialization. However, a consistency check ensures that both algorithms agree with each other, to remove anomalous events. At the fiducial radius, the PE-based algorithm is estimated to have a resolution of 30 mm to 45 mm within the WIMP PE-range.

3. Background model and mitigation

The background model is summarized in Table 1. For each source, a control region (CR) is defined to select that background in data; the background models are studied in the CRs and used to predict the number of events in the WIMP PE range after the CR selection cuts (N_i^{CR}) and in the ROI after all WIMP search cuts (N_i^{ROI}). Cuts were tuned on these models to bring N_i^{ROI} from each source below some target value, chosen for a total $\sum_i N_i^{ROI} < 1$.

As demonstrated in Figure 1, PSD efficiently mitigates ER backgrounds. Most Chereknov events have F_{prompt} above the ROI (see Figure 3). Chernekov in the LGs is further discriminated by removing events with light highly concentrated in a single channel, while Cherenkov in the FGs is tagged by the NV. Radiogenic neutrons are measured *in situ* by searching for neutron-induced NRs followed by high energy γ-ray-induced ERs after the neutron captures. This

Table 1. The expected number of background events in each control region between 95 PE to 200 PE (N_i^{CR}) and in the WIMP-search region of interest after all cuts (N_i^{ROI}).

	Source	N_i^{CR}	N_i^{ROI}
β/γ's	ERs	2.44×10^{9}	0.03 ± 0.01
	Cherenkov	$<3.3\times10^{5}$	<0.14
n's	Radiogenic	6 ± 4	$0.10^{+0.10}_{-0.09}$
	Cosmogenic	<0.2	<0.11
α's	AV surface	<3600	<0.08
	Neck Flow Guide	28^{+13}_{-10}	$0.49^{+0.27}_{-0.26}$
	Total	N/A	$0.62^{+0.31}_{-0.28}$

estimate is consistent with simulations normalized to *ex situ* assays and neutron flux calculations. These backgrounds are reduced by the fiducial cut. Cosmogenic neutrons are rare due to the low muon flux at SNOLAB, with an overburden equivalent to 6 km of water. Backgrounds are further reduced by tagging events in which muon-induced Cherenkov light is seen in the MV.

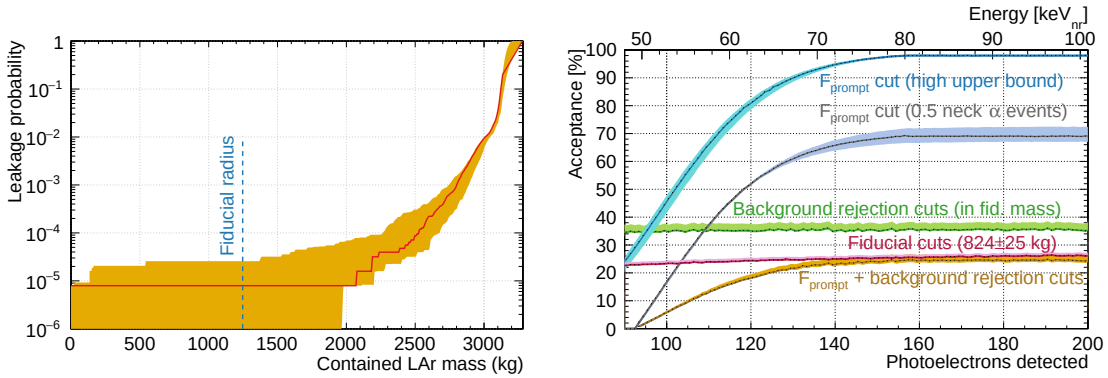

Figure 2. (Left) The AV surface α-decay leakage probability vs. the LAr mass within a fiducial radius. (Right) The WIMP acceptance vs. PE detected after various sets of cuts are applied.

As shown in Figure 2, α-decays on the AV surface are removed by the fiducial cut. The dominant background comes from α-decays in the neck. If an α-particle scintillates in a film of LAr on a FG surface, most light may be lost, causing the events to appear at lower PE. Due to the geometry of the neck, the number of PE detected and the reconstructed z-coordinate are correlated, creating features at high-PE that can be used to measure the rate of these events. Since they are high energy events that appear at low PE, they have higher $\mathrm{F_{prompt}}$ than NRs. They are also reduced by vetoing events with very early or excessive light in the PMTs in the GAr layer, or significant disagreement between both position reconstruction algorithms.

4. Results

The WIMP acceptance after all cuts is shown in Figure 2. The biggest loss of acceptance comes from cuts used to discriminate α-decays in the neck; efforts are underway to use multivariate analyses to more efficiently discriminate against them. After all cuts are applied, 0 events remain in the WIMP ROI, as shown in Figure 3. At 90 % C. L., this analysis excludes spin-independent WIMP-nucleon scattering cross sections above $3.9\times10^{-45}\mathrm{cm}^2$ ($1.5\times10^{-44}\mathrm{cm}^2$) for WIMPs with a mass of 100 $\mathrm{GeV/c}^2$ (1 $\mathrm{TeV/c}^2$), assuming the standard WIMP halo, as shown in Figure 3.

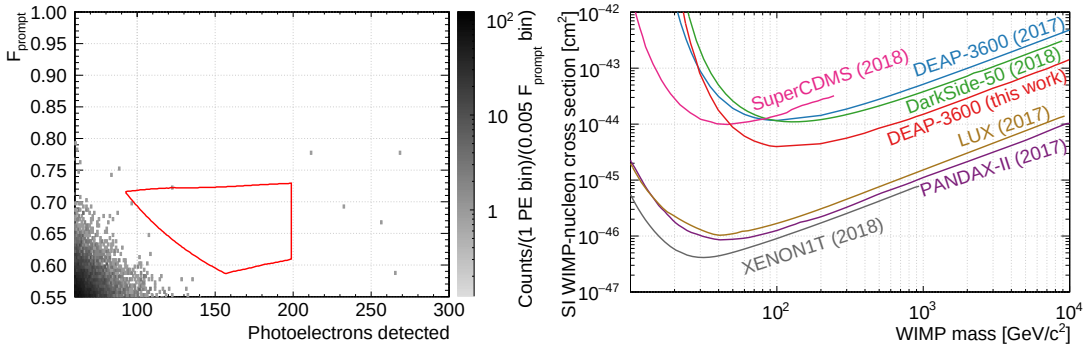

Figure 3. (Left) Events remaining after cuts, with the ROI in red. (Right) 90% C. L. upper limits on the spin-independent WIMP-nucleon cross sections from the present [3] and past analyses [2], SuperCDMS [7], DarkSide-50 [8], LUX [9], PANDAX-II [10], and XENON1T [11].

Acknowledgments

This work is supported by the Natural Sciences and Engineering Research Council of Canada, the Canadian Foundation for Innovation (CFI), the Ontario Ministry of Research and Innovation (MRI), and Alberta Advanced Education and Technology (ASRIP), Queen's University, University of Alberta, Carleton University, the Canada First Research Excellence Fund, the Arthur B. McDonald Canadian Astroparticle Physics Research Institute, DGAPA-UNAM (PAPIIT No. IA100118) and Consejo Nacional de Ciencia y Tecnología (CONACyT, Mexico, Grants No. 252167 and A1-S-8960), the European Research Council (ERC StG 279980), the UK Science & Technology Facilities Council (STFC) (ST/K002570/1 and ST/R002908/1), the Leverhulme Trust (ECF-20130496). Studentship support by the Rutherford Appleton Laboratory Particle Physics Division, STFC and SEPNet PhD is acknowledged. We thank SNOLAB and its staff for support through underground space, logistical and technical services. SNOLAB operations are supported by CFI and the Province of Ontario MRI, with underground access provided by Vale at the Creighton mine site. We thank Compute Canada, Calcul Québec, the Centre for Advanced Computing at Queen's University, and the Computational Centre for Particle and Astrophysics (C2PAP) at the Leibniz Supercomputer Centre (LRZ) for providing the computing resources required for this work.

References

[1] Amaudruz P A *et al.* (DEAP Collaboration) 2019 *Astropart. Phys.* **108** 1–23

[2] Amaudruz P A *et al.* (DEAP Collaboration) 2018 *Phys. Rev. Lett.* **121** 071801

[3] Ajaj R *et al.* (DEAP Collaboration) 2019 *Phys. Rev. D* **100** 022004

[4] Akashi-Ronquest M *et al.* 2015 *Astropart. Phys.* **65** 40–54

[5] Amaudruz P A *et al.* (DEAP Collaboration) 2019 *Nucl. Instrum. Methods Phys. Res. A* **922** 373–384

[6] Cao H *et al.* (SCENE Collaboration) 2015 *Phys. Rev. D* **91** 092007

[7] Agnese R *et al.* (SuperCDMS Collaboration) 2018 *Phys. Rev. Lett.* **120** 061802

[8] Agnes P *et al.* (DarkSide Collaboration) 2018 *Phys. Rev. D* **98** 102006

[9] Akerib D *et al.* (LUX Collaboration) 2017 *Phys. Rev. Lett.* **118** 021303

[10] Cui X *et al.* (PandaX-II Collaboration) 2017 *Phys. Rev. Lett.* **119** 181302

[11] Aprile E *et al.* (XENON1T Collaboraiton) 2018 *Phys. Rev. Lett.* **121** 111302 arXiv: 1805.12562